

## Aberystwyth University

### Towards characterising rhyolitic tephra layers from New Zealand with rapid, non-destructive $\mu$ -XRF core scanning

Peti, Leonie; Augustinus, Paul C.; Gadd, Patricia S.; Davies, Sarah

*Published in:*  
Quaternary International

*DOI:*  
[10.1016/j.quaint.2018.06.039](https://doi.org/10.1016/j.quaint.2018.06.039)

*Publication date:*  
2019

*Citation for published version (APA):*

Peti, L., Augustinus, P. C., Gadd, P. S., & Davies, S. (2019). Towards characterising rhyolitic tephra layers from New Zealand with rapid, non-destructive  $\mu$ -XRF core scanning. *Quaternary International*, 514, 161-172.  
<https://doi.org/10.1016/j.quaint.2018.06.039>

#### General rights

Copyright and moral rights for the publications made accessible in the Aberystwyth Research Portal (the Institutional Repository) are retained by the authors and/or other copyright owners and it is a condition of accessing publications that users recognise and abide by the legal requirements associated with these rights.

- Users may download and print one copy of any publication from the Aberystwyth Research Portal for the purpose of private study or research.
- You may not further distribute the material or use it for any profit-making activity or commercial gain
- You may freely distribute the URL identifying the publication in the Aberystwyth Research Portal

#### Take down policy

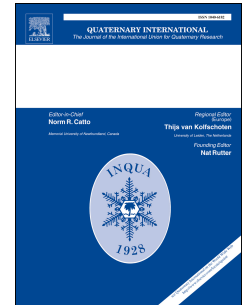
If you believe that this document breaches copyright please contact us providing details, and we will remove access to the work immediately and investigate your claim.

tel: +44 1970 62 2400  
email: [is@aber.ac.uk](mailto:is@aber.ac.uk)

# Accepted Manuscript

Towards characterising rhyolitic tephra layers from New Zealand with rapid, non-destructive  $\mu$ -XRF core scanning

Leonie Peti, Paul C. Augustinus, Patricia S. Gadd, Sarah J. Davies



PII: S1040-6182(18)30252-0

DOI: [10.1016/j.quaint.2018.06.039](https://doi.org/10.1016/j.quaint.2018.06.039)

Reference: JQI 7499

To appear in: *Quaternary International*

Received Date: 4 March 2018

Revised Date: 19 May 2018

Accepted Date: 26 June 2018

Please cite this article as: Peti, L., Augustinus, P.C., Gadd, P.S., Davies, S.J., Towards characterising rhyolitic tephra layers from New Zealand with rapid, non-destructive  $\mu$ -XRF core scanning, *Quaternary International* (2018), doi: 10.1016/j.quaint.2018.06.039.

This is a PDF file of an unedited manuscript that has been accepted for publication. As a service to our customers we are providing this early version of the manuscript. The manuscript will undergo copyediting, typesetting, and review of the resulting proof before it is published in its final form. Please note that during the production process errors may be discovered which could affect the content, and all legal disclaimers that apply to the journal pertain.

Towards characterising rhyolitic tephra layers from New Zealand with rapid, non-destructive  $\mu$ -XRF core scanning

Leonie Peti<sup>1\*</sup>, Paul C. Augustinus<sup>1</sup>, Patricia S. Gadd<sup>2</sup>, Sarah J. Davies<sup>3</sup>

<sup>1</sup> School of Environment, University of Auckland (New Zealand)

<sup>2</sup> Australian Nuclear and Science Technology Organisation, Sydney (Australia)

<sup>3</sup> Department of Geography and Earth Sciences, Aberystwyth University (Wales, UK)

\* Corresponding Author: Leonie Peti, lpet986@aucklanduni.ac.nz; School of Environment, The University of Auckland, Private Bag 92019, Auckland 1142 New Zealand

## Abstract

Tephra layers are of importance for the construction of reliable age control in late Quaternary paleoenvironmental and volcanic hazard studies, especially in volcanically-active settings such as the North Island of New Zealand. However, their identification involves time-consuming and destructive processing steps, making the application of non-destructive  $\mu$ -XRF core scanners potentially advantageous for tephra identification. Here, we investigate the potential of the Itrax  $\mu$ -XRF core scanner to differentiate between rhyolitic tephra layers sourced from various northern New Zealand rhyolitic volcanic centres deposited in maar lakes of the Auckland Volcanic Field. In their macroscopic form these tephra layers are usually visibly distinct when surrounded by a dark, organic-rich sediment matrix, although their attribution to source volcanic centre and eruption typically requires examination of their mineral assemblages, combined with chemical fingerprinting of the rhyolite glass shards. We demonstrate that  $\mu$ -XRF core scanning of rhyolitic tephra layers from the Taupo Volcanic Zone and Tuhua Volcanic Centre can also allow identification, and sometimes differentiation, of the tephra using  $\mu$ -XRF-derived elemental counts, especially high Si, K, Ca and very low Br and Ti. Different rhyolite tephra layers vary in their relative abundances of major, minor and trace elements as is evident from electron microprobe and LA-ICP-MS analyses of their glass shards. Mo-tube based  $\mu$ -XRF cannot detect Na nor Mg and is of lower reliability for the lighter elements (Ca, Al) which play an important role in traditional tephra fingerprinting. Nevertheless, we are able to demonstrate that  $\mu$ -XRF core scanning data can distinguish between previously identified tephra layers using multivariate statistics. Furthermore, the study emphasises the need for a standard protocol for  $\mu$ -XRF core scanning of tephra layers for this approach to be more widely applicable,

especially to aid or be a substitute for conventional geochemical approaches used for tephra fingerprinting.

Keywords: Itrax; Tephra; Multivariate Statistics; Principal Component Analysis; Discriminant Factor Analysis; Auckland Volcanic Field, New Zealand

## 1 Introduction

Lake sediment-based reconstructions of late-Quaternary environmental change are only useful if based on reliable chronologies. Nevertheless, many of the changes in climatic and environmental conditions of interest occurred more than 50,000 years ago and/or cannot be dated by the radiocarbon technique. Fortunately, volcanic eruptions produce tephra that are deposited as layers both proximal and distal to volcanic centres and serve as time markers that aid the development of reliable chronologies (Shane, 2000; Lowe, 2011; Lane et al., 2017). This is the science of tephrochronology which is an important method for dating late Quaternary lake sediment sequences in northern New Zealand (Molloy et al., 2009).

Tephrochronology involves the unambiguous identification of tephra that are sometimes spread over large areas distal from the eruption site. Eruptions are effectively instantaneous events where they are preserved in the geological record so that the resulting tephra layers are isochrons. If the eruption has been dated by some means, the same age can be attributed to the widely-distributed tephra layers produced thereby underlining the importance of tephra to dating sediment-based records of past environmental change, as well as in volcanic hazard analysis (Shane, 2000; Lowe et al., 2008; Lowe, 2011).

To be able to establish reliable correlations between tephra layers encountered at different locations distal to the source and to proximal eruptive deposits, geochemical characterisation of the tephra is necessary and termed “fingerprinting”. Traditionally, tephra layers are fingerprinted geochemically and petrographically based on electron probe microanalysis (EPMA; for major element oxide composition), LA-ICP-MS (Laser ablation inductively coupled plasma mass spectrometry; for minor and trace elements) of volcanic glass and microscopic investigation of the diagnostic mineral assemblage (e.g., Shane, 2000; 2005; Shane and Smith, 2000; Lowe et al., 2008; 2013; Dugmore and Newton, 2012; Lane et al., 2017). However, this process is destructive and time consuming, thereby complicating the use of tephra as known-age isochrons in lake sediment sequences.



In contrast,  $\mu$ -XRF scanning of sediment cores is fast, non-destructive and needs virtually no sample preparation (e.g., Croudace et al., 2006; Thomson et al., 2006; Croudace and Rothwell, 2010). Sediment-based records of past environmental change often routinely undergo  $\mu$ -XRF scanning to obtain continuous time-series of geochemical data for elements with an atomic number  $Z \geq 13$  (Al to U). The geochemical data required for tephra recognition and identification/fingerprinting are collected automatically in the  $\mu$ -XRF process. Hence, the potential advantages of being able to rapidly and reliably identify tephra using  $\mu$ -XRF core scanners are clear.

Prior research into the potential of using  $\mu$ -XRF core scanners as a tephrochronological aid has focussed on the ability to locate cryptotephra invisible to the un-aided eye (e.g., Balascio et al., 2015), or to identify tephra in lake sediment cores (Kylander et al., 2012). The latter authors do not recommend the use of  $\mu$ -XRF core scanning data as a tool for tephra identification based on basaltic and low-concentration rhyolitic tephra layers in sediment cores from the Faroe Islands. However, improvements in the Itrax detector system and the abundance of macroscopic (visible) tephra layers with distinctive chemistries in New Zealand (Lowe et al., 2008) require a more thorough investigation of the potential of  $\mu$ -XRF core scanning techniques for reliable tephra identification.

This study focuses on tephras in lake sediment cores retrieved from maars in the Auckland Volcanic Field (AVF; northern New Zealand) which unites outstanding high-resolution and finely-laminated records of late-Quaternary environmental change with well-preserved tephra deposits from a wide variety of volcanic systems (andesitic, basaltic, and rhyolitic).

## 2 The AVF

The AVF consists of about 53 basaltic volcanoes (Lindsay et al., 2011). Thirteen of these are explosion craters, called maars, formed by phreatomagmatic eruptions (Cas and Wright, 1988; Smith, 1989). All maar craters referred to in this study (Fig. 1) have hosted a lake for varying durations over the past ca. 250 ka (Molloy et al., 2009). Lake Pupuke is the only maar in the AVF which has not been in-filled and/or breached and contains an extant lake (Augustinus et al., 2006; 2008; Stephens et al., 2012; Newnham et al., 2018). The extant and in-filled maar lakes mostly have steep crater rims combined with deep lacustrine basins with small width to depth ratios resulting in excellent preservation potential of sediment and tephra derived from both tephra fall and reworking from the steep subaqueous crater rim slopes (Molloy et al., 2009; Zawalna-Geer et al., 2016).

The AVF maar lake sediment sequences often show pronounced fine laminations recording changes in regional climate and environmental conditions, possibly even at annual to decadal resolution

(Pepper et al., 2004; Augustinus et al., 2006; Striewski et al., 2013). For the past ca. 46 ka, good age control was largely established based on identification of geochemically-distinct, well-dated and well-preserved tephra (volcanic ash) isochrons (Shane, 2000; Molloy et al., 2009; Augustinus et al., 2011). This dependence on tephra layers for AVF maar lake sediment sequence chronology development highlights the need for fast and reliable identification of tephra in lake sediment cores proximal or distal to tephra-producing volcanic zones.

*Figure 1 about here, over one column*

## 2.1 Tephra records from the AVF maar crater lakes

The North Island volcanic centres (VC) that contribute rhyolitic and andesitic tephra to the Auckland maar lakes are located south of Auckland: the Okataina (OVC), Taupo (TVC), Egmont volcano (Eg; Taranaki) and Tongariro (TgVC) volcanic centres, as well as the smaller Tuhua VC (Mayor Island) to the SE. In addition, the c. 53 volcanoes in the AVF produced basaltic tephra which are dispersed locally (Fig. 1). Rhyolitic, basaltic and andesitic tephra from these centres have frequently reached the AVF maar lakes (Molloy et al., 2009; Zawalna-Geer et al., 2016), highlighting their value as known-age isochronous marker layers for both chronology development and correlation of the sediment sequences between maars. Furthermore, volcanic hazard assessment for the AVF basaltic volcanoes rely on identification of basaltic tephra layers contained in the maar lake sequences although their timing has largely been constrained by the bracketing known age rhyolitic tephra (Molloy et al., 2009; Hopkins et al., 2015). However, new approaches using  $^{40}\text{Ar}/^{39}\text{Ar}$  dating of the basaltic lava flows from the source AVF volcanoes correlated to basaltic tephra deposits (Hopkins et al., 2017; Leonard et al., 2017), zircon double-dating (Danišik et al., 2012), and meteoric  $^{10}\text{Be}$  and magnetic paleointensity studies of the maar lake sediments (Nilsson et al., 2011) have the ability to dramatically improve the chronology of the sequences beyond the  $^{14}\text{C}$ -dating- method limit of c. 60 cal ka under favourable conditions.

In this study, we investigate the scanning  $\mu$ -XRF characteristics of rhyolite tephra layers in sediment cores from five AVF maar paleolakes: Onepoto Domain, Orakei Basin, Panmure Basin, Hopua Crater, and Pukaki Lagoon; plus one extant lake, Pupuke (Fig. 1). Only rhyolite tephra layers were used as they are the most widely-dispersed and widely-used tephrochronological deposits in New Zealand.

## 3 Material and methods

### 3.1 Rhyolitic tephra layers

The tephra records documented in sediment cores from Hopua maar, Lake Pupuke and the Orakei Basin core collected in 2007, Pukaki and Onepoto maars are presented in Table 1. Figures 2 and 3 in Molloy et al. (2009) present the studied rhyolitic tephra layers in stratigraphic context of the Auckland Volcanic Field maar lake records. This study focusses only on macroscopic rhyolitic tephra layers which have previously been identified through EPMA glass chemical composition (Molloy et al., 2009 and unpublished data by Zawalna-Geer). Table 1 summarises the names, source volcanic centres and dominant mineralogy of the 13 rhyolitic tephra layers investigated in this study.

Table 1: Overview over investigated rhyolitic tephra layers in this study following Lowe et al. (2008) and Molloy et al. (2009).

Name	Ferromagnesian mineralogy <sup>2</sup>	Centre <sup>1</sup>
Tuhua	aeg > cpx > opx ± aen ± rie ± hb ± olv(fa) ± tuh	TUVC
Mamaku	hb > opx >> ± cgt	OVC
Rotoma	cgt > hb	OVC
Opepe	opx >> cpx	TVC
Waiohau	opx > hb	OVC
Rotorua	bio > opx > hb	OVC
Okareka	bio	OVC
Kawakawa/Oruanui	opx > hb	TVC
Okaia	opx > hb	TVC
Hauparu	hb, opx	OVC
Maketu	hb > opx	OVC
Tahuna	opx > hb	TVC
Rotoehu	bio = hb = cgt	OVC

<sup>1</sup>TUVC: Tuhua Volcanic Centre (Mayor Island); OVC: Okataina Volcanic Centre; TVC: Taupo Volcanic Centre

<sup>2</sup> aeg: aegirine; aen: aenigmatite; bio: biotite; cgt: cummingtonite; cpx: clinopyroxene; hb: hornblende; olv(fa): olivine (fayalite); opx: orthopyroxene; tuh: tuhualite. ± indicates may or may not be present.

## 3.2 Methods

### 3.2.1 $\mu$ -XRF Core Scanning

The sediment cores were scanned with three different Itrax  $\mu$ -XRF Core Scanners (Cox Analytical Systems, Gothenburg, Sweden) at Aberystwyth University (AU, UK), the Australian Nuclear and Science Technology Organisation (ANSTO, Australia), and The University of Auckland (UOA, New Zealand) with settings specified in Table 2. Each scan resulted in an optical image, a radiograph and single dispersive energy spectra for each interval measured along the core profile. Integrated peak area integrals for each element are calculated from the spectra which are then output as X-ray fluorescence (XRF) count data (Croudace et al., 2006; Thomson et al., 2006; Croudace and Rothwell, 2010).

Table 2: Overview of  $\mu$ -XRF scanning locations and conditions used in this study

Site	Location of scan	Year of scan	X-ray tube	Voltage	Current	XRF exposure time	Step size
Pupuke	AU <sup>1</sup>	2008	Mo	30 kV	20 mA	10 s	200 $\mu$ m
Hopua	AU	2008	Mo	30 kV	45 mA	10 s	200 $\mu$ m
Panmure	AU	2010	Mo	30 kV	45 mA	10 s	200 $\mu$ m
Onepoto	ANSTO <sup>2</sup>	2013	Mo	30 to 55 kV	50 to 55 mA	10 s	1000 $\mu$ m
Orakei	UOA <sup>3</sup>	2017	Mo	30 kV	55 mA	10 s	1000 $\mu$ m
Hopua	UOA	2017	Mo	30 kV	55 mA	10 s	1000 $\mu$ m
Panmure	UOA	2017	Mo	30 kV	55 mA	10 s	1000 $\mu$ m
Onepoto	UOA	2017	Mo	30 kV	55 mA	10 s	1000 $\mu$ m

<sup>1</sup>: Aberystwyth University; <sup>2</sup>: Australian Nuclear Science and Technology Organisation; <sup>3</sup>: University of Auckland

### 3.2.2 Data Treatment

To correct for variability in sediment water, organic matter content and grain size, as well as X-ray tube ageing, all elemental peak intensities have been normalised to the sum of incoherent and coherent scattering (inc+coh; Löwemark et al., 2011; Kylander et al., 2012). Unless otherwise stated, element "X" refers to elemental peak areas normalised by inc+coh (Fig. 2).

*Figure 2 about here, landscape over full page*

As an initial step, we examined the kernel density estimation (KDE) of the distribution of elemental counts of Al, Si, P, S, Cl, K, Ca, Ti, V, Mn, Fe, Ni, Zr, Br, Rb, Sr, Zr (all normalised to inc+coh) and inc+coh (Fig. 3, 4). KDE estimates the probability density function of the variable in question and can be understood as a smoothed version of a histogram.

Most elements follow approximately log-normal distributions. Some elements display bimodal distributions within the general shape of a log-normal distribution (Fig. 3). The bimodality was largely preserved after log-ratio transformation with many elements showing skewed distributions to various degrees (Fig. 3, 4). A condition of the statistical tests described below is normal distribution of the data (Zelterman, 2015). To obtain roughly normally distributed data the normalised counts have been log-ratio transformed.

The bimodality and skewed distributions (Fig. 3) partly result from mixing  $\mu$ -XRF scanning data from different Itrax scanners using different detector generations (Fig. 4, Table 2). The maximum counts a new detector (i.e., the Itrax at the University of Auckland) can record are several times higher than those of the older detector (i.e., the Itrax at the Aberystwyth University in 2008). Despite normalizing the data by inc+coh, substantial differences in the numerical counts remain (Fig. 4). These differences between detectors have a stronger influence on the distribution shape than actual differences in element "X" between the tephra layers, thereby causing a skewed or multimodal shape.  $K_{\text{norm}}$ ,  $\text{Ca}_{\text{norm}}$  and  $\text{Sr}_{\text{norm}}$  are presented in Fig. 4 as an example separated by tephra layer (colour) and Itrax scanner (line pattern). Although differences between the tephra layers can generally be observed, differences between the Itrax scanners become apparent too. For example, the distribution of the Tahuna tephra reaches its respective peaks of  $K_{\text{norm}}$  (Fig. 4) in the lower end of the entire distribution in the  $\mu$ -XRF data from ANSTO and in the middle part in the data from UOA. However, the Mamaku tephra is consistently recorded with overlapping highest density of the  $\text{Ca}_{\text{norm}}$  and  $\text{Sr}_{\text{norm}}$  distribution in  $\mu$ -XRF data from UOA and AU. Additionally, it becomes clear that different tephra layers show distinct peaks in the density distribution of normalised  $\mu$ -XRF counts, thus pointing to the possibility of geochemical differentiation between tephra layers based on  $\mu$ -XRF counts.

For further analyses, the tephra layers have been split into pre-Kawakawa/Oruanui tephra (KOT, inclusive) layers and post-KOT layers. The KOT is the product of a caldera-forming super eruption  $25,360 \pm 160$  cal yr BP (Pillans et al., 1993; Vandergoes et al., 2013) that produced widely-dispersed tephra.

Data from three different Itrax  $\mu$ -XRF core scanners

Mixing  $\mu$ -XRF scanning data from different Itrax scanners used with different detector generations and different scanning settings cause complications for numerical analyses which cannot be corrected for easily. Hence, we split the dataset by core scanner location and only proceed with data from the ANSTO Itrax (for pre-KOT) and the UOA Itrax (for post-KOT), separately for further multivariate statistical analyses. The decision to exclude the data from the AU Itrax was motivated by the smaller number of scanned tephra layers, the older detector<sup>1</sup> used with lower sensitivity for lighter elements and different scanning settings from the ANSTO and UOA Itrax scans (see Table 1).

The logarithm of "0" is not defined. Hence, special care must be taken when applying log-transformation to data including "0". Only elements which have been measured in all scanning routines are kept for interpretation to avoid introducing artificial 0-values. Additionally, measurements of some elements of low abundance and/or low detection limit in the  $\mu$ -XRF technique (e.g., Al) result in "0" in many measurements. Cuven et al. (2007) recommended removing all elements that include more than 30% of 0-values. All measurements that still include one or more 0-values after this step must also be removed, resulting in the possible removal of the thinner tephra layers that are represented by fewer  $\mu$ -XRF data points. Hence, we chose to remove all elements that include more than 10% of 0-values and remove the few remaining measurements including 0-values.

*Figure 3 about here, landscape over full page*

*Figure 4 about here, landscape over full page*

Data transformation

Elemental counts obtained from  $\mu$ -XRF scanning are compositional data consisting of proportions summing to a constant and are non-negative (Aitchison, 1986). Hence, the variation of one component of the total (i.e., an element "X" whether it can be detected by the Itrax or not) influences the amount of all other elements. This unit-sum constraint possibly results in incorrect inference when improperly incorporated into the statistical analyses and is well known in the geostatistical community (e.g., Lowe et al., 2017). Aitchison (1986) has developed a simple approach to removing this constraint by applying log-ratio transformation where the natural logarithm of ratios between two components of the sum are computed. Note, however, that all the data

---

<sup>1</sup> Note that the Aberystwyth University Itrax detector has been upgraded in 2008 and 2015 with improved sensitivity.

presented here are ratios because they have been normalized by inc+coh. Many authors favour log-ratio transformation (e.g., Weltje and Tjallingii, 2008; Weltje et al., 2015; Martin-Puertas et al., 2017) whereas others question its use (e.g., Pearce et al., 2008; Feng et al., 2014). Lowe et al. (2017) point out that any statistical analyses should ideally be performed on transformed and un-transformed data and if transformation alters the results obtained caution has to be taken with the use of the dataset. Hence, all the following statistical approaches applied to the rhyolite tephra  $\mu$ -XRF data involve log-ratio transformed and raw (normalised) data to compare results. The results of both approaches are very similar giving confidence to the presented  $\mu$ -XRF-based geochemical fingerprinting approach.

#### Principal component analysis

Principal component analysis (PCA) finds the direction of highest variance within the multivariate data and fits the first principal component (PC) along this direction. Each subsequent component describes a subsequently smaller amount of variance of the original dataset and is oriented orthogonally to the prior component (e.g., Zeltermann, 2015). In the resulting biplot, the proximity of the data points to each other suggests a strong similarity between the measurements, while proximity between the elemental loadings and data points emphasises the correlation between the respective type of material (sediment or certain tephra layer) and the measured elements (e.g., Zeltermann, 2015).

PCA has been applied to  $\mu$ -XRF scanning results from the Onepoto core measured at ANSTO (Fig. 7A),  $\mu$ -scanning results from the Hopua core measured at the University of Auckland (Fig. 7B), pre-KOT rhyolitic tephra layers in the Onepoto core (measured at ANSTO (Fig. 7A), and post-KOT rhyolitic tephra layers in the Hopua and Panmure cores (measured at University of Auckland) (Fig. 7B).

#### Discriminant function analysis

Linear discriminant analysis (LDA) is a subclass among discriminant function analyses that determines a linear combination of independent variables (here elemental intensities) leading to a single transformed variable by which *a-priori* classified, mutually exclusive groups (here tephra layers classified by EPMA data) may be discriminated (e.g., Zeltermann, 2015). The first linear discriminant function (LD) achieves the largest separation between the pre-classified groups similar to the 1<sup>st</sup> PC. LDA has been successfully applied to EPMA data of tephra layers in New Zealand to discriminate between previously classified tephra layers and test the applicability to identify

subsequently encountered tephra layers (Stokes and Lowe, 1988; Stokes et al., 1992; Shane and Froggatt, 1994; Cronin et al., 1996).

## 4 Results and Discussion

### 4.1 Geochemical distinction between rhyolitic tephra layers and sediment matrix

Variability in elemental counts obtained by  $\mu$ -XRF scanning clearly shows the rhyolitic tephra layers in sediment cores (Fig. 4), which works well when the intervening sediment is organic matter-rich resulting in marked geochemical contrast between lake sediment and tephra layers. Thinner tephra layers are more difficult to locate by  $\mu$ -XRF scanning than thicker tephra layers. Practically, there is no clear minimum thickness for a tephra layer in order to be located and identified by this technique. If a strong contrast in chemical composition to other tephra layers exists even  $<200\ \mu\text{m}$  tephra layers may be identified by this technique in the future. However, for statistical reliability a minimum thickness of c. 1 mm is favourable for this technique.

PCA of normalised elemental counts highlights the power to differentiate between lacustrine/marine sediment and rhyolitic tephra layers based on  $\mu$ -XRF core scanning data (Fig. 5).

During  $\mu$ -XRF scanning, Si, K and Ca are consistently elevated in the rhyolitic tephra layers with respect to the sediment matrix. The high counts of the latter elements are consistent with the geochemistry of the rhyolitic tephra (Winter, 2001; Lowe et al., 2008). Furthermore, most rhyolitic tephra layers are positively correlated to Mn, Rb and Sr as identified by PCA (Fig. 5). In contrast, rhyolitic tephra layers are always relatively depleted in Br which is consistent with Br being an indicator for organic rich sediment (Davies et al., 2015; Rothwell and Croudace, 2015; note the correlation of Br with lacustrine sediment in all PCA results in Fig. 5). It is striking that Zn, Rb, Sr and Zr vary in their behaviour between discrete tephra layers of different ages, e.g., Zr is high in the Maketu, Hauparu and Tuhua layers compared to the amounts in the encapsulating sediment whereas Sr is elevated in most tephra layers but depleted in the Tuhua layer (Fig. 4).

The  $\mu$ -XRF presented data shows that tephra layers sourced from the TVC are chemically distinct from those sourced from the OVC and from those erupted by the TUV as has been observed in conventional tephrochronological methods (e.g., Lowe et al., 2017). This finding provides confidence that  $\mu$ -XRF core scanners have the potential to fingerprint rhyolitic tephra layers to their source volcanic centre.

*Figure 5 about here, landscape over full page*



287

## 288 4.2 Multivariate geochemical discrimination between the rhyolitic tephra layers

289 Most discrete rhyolitic tephra layers such as the Rotoehu, Tahuna, Maketu, Hauparu, Okaia,  
 290 Okareka, Waiohau, Rotoma and Tuhua tephra are strongly depleted in Ti whereas the  
 291 Kawakawa/Oruanui (KOT) and Rotorua tephra show no discernible difference in levels of Ti  
 292 compared with that of the sediment matrix. Only the Mamaku and Tuhua tephra are enriched in Fe  
 293 (Fig. 2B). Tahuna, Maketu, Hauparu and Tuhua tephra are enriched in Zn compared to the amounts  
 294 in the sediment matrix and the rhyolite tephra layers, except for Okareka and Mamaku tephra, are  
 295 enriched in Rb (Fig. 2). Tuhua is the only tephra clearly depleted in Sr while all other rhyolitic tephra  
 296 layers examined are enriched in Sr to various degrees. The Maketu, Hauparu, KOT, Rotorua,  
 297 Waiohau and Tuhua tephra layers are strongly enriched in Zr. All the other tephra layers show no or  
 298 very minor differences in Zr levels between the sediment and the tephra (Fig. 2).

299 Comparing only the tephra layers to one another indicates that the different layers form different  
 300 clusters in a biplot (Fig. 6) and linear discriminant analysis (Fig. 7). The thin tephra layers (Okaia,  
 301 Hauparu, Tahuna, Mamaku, Opepe and Waiohau) are not easily identifiable due to the limited  
 302 number of data points available due to their thickness. High-resolution (200  $\mu\text{m}$ )  $\mu\text{-XRF}$  scans over  
 303 multiple lateral positions of thin tephra layers may increase the possibility of identifying the thick  
 304 tephra layers.

## 305 Pre-KOT rhyolite tephra

306 PCA and LDA enabled identification of the largest difference between Rotoehu and the four other  
 307 pre-KOT rhyolitic tephra layers (Fig. 6A, 7A). Separation along PC1 and LD1 is mostly achieved with  
 308 Rotoehu tephra which is relatively enriched in Si, Sr, K and Rb, whilst displaying relative depletion in  
 309 Ca, Zn, Fe, Cl and Mn. PC2 and LD2 achieve a clear separation between the Maketu/Hauparu and  
 310 Tahuna/Okaia tephra, respectively, with the former being relatively enriched in Ca, Rb, Si, Ti and Fe  
 311 and the latter relatively enriched in Mn, Sr and K (Fig. 6A, 7A). Along LD2, the Maketu, Hauparu and  
 312 Rotoehu tephra form one cluster (Fig. 6A, 7A) corresponding to the OVC-source of these three  
 313 tephra layers (Table 1, Fig. 1). The other cluster along LD2 is formed by Okaia and Tahuna tephra and  
 314 corresponds to their TVC source (Fig. 1, 7A). Fig. 6A shows scattered outliers, especially in the lower  
 315 left corner where Tahuna and Okaia tephra chemistries mix (Fig. 7A). The observed wide scatter of  
 316 data points emphasizes the need for more elemental data points, especially for the thinner tephra  
 317 layers to better constrain the tephra-source defined clusters and remove outliers.

## 318 Post-KOT rhyolite tephra

PCA and LDA plots show clear elemental differentiation between the Tuhua and all other post-KOT tephra (Fig. 2B, 5B) which is consistent with it being the only tephra from the Tuhua Volcanic Centre examined in this study and its contrasting composition to the others as noted in earlier studies based on glass shard EPMA data (e.g., Lowe et al., 2008). Tuhua tephra is relatively enriched in Fe, Zn, Zr, Y, and Mn and depleted in Sr (Fig. 2B). Hence, PC1 and LD1 allow separation of the Mayor Island-sourced tephra from the remaining post-KOT rhyolitic tephra layers. Rotoma, Rotorua and Opepe tephra each have sufficient data points to produce well-defined clusters in the PCA bi-plot (Fig. 2B). PC2 largely allows elemental discrimination between Rotorua (relatively enriched in Ca) and Opepe tephra (Fig. 2B). The same trend is visible, but clearer, in the LDA where LD3 achieves separation between TVC and OVC+TU sourced rhyolitic post-KOT tephra layers (Fig. 5B).

*Figure 6 about here, landscape over full page*

*Figure 7 about here, one and a half page width*

#### 4.3 Bivariate scatterplots

Using multivariate statistics, a suite of bivariate scatterplots showing the clearest separation of individual tephra layers can be produced and is supplemented by typical bivariate scatterplots for rhyolitic tephra (e.g., SiO<sub>2</sub> vs. K<sub>2</sub>O; Shane, 2000) identification based on traditional EPMA data in Fig. 8.

#### Pre-KOT rhyolite tephra

All pre-KOT elemental scatterplots (Fig. 8A) show the outliers of the Rotoehu, Maketu, Hauparu and Okaia tephra layers at a significant distance from their respective clusters as was observed in the PCA biplots (Fig. 6A). A standard bivariate plot used by the tephrochronological community for differentiating and fingerprinting tephra layers to source, and possibly event of an eruption, is SiO<sub>2</sub> vs. K<sub>2</sub>O (e.g., Shane, 2000). However, the equivalent  $\mu$ -XRF scanning of Si vs. K plot of log-transformed  $\mu$ -XRF core scanning data only achieves clear separation between Okaia+Tahuna vs. Rotoehu+Maketu+Hauparu tephra (Fig. 8A). Bivariate plots of Ca vs. K, Fe vs. Ca, Si vs. Zn, Sr vs. Ca and Rb vs. Sr (Fig. 8A) show a clear separation between the Maketu and Rotoehu tephra. The lower number of  $\mu$ -XRF data points for the Okaia and Tahuna tephra as well as the large variance in  $\mu$ -XRF elemental counts complicate the recognition of a clear cluster corresponding to their mean

count values of the latter elements. It is not possible to conclude whether the data points distal from the centre of the cluster are outliers due to scanning or core condition (e.g., small amounts of foreign material mixed with the tephra layer not visible at the core surface) or if these tephra layers exhibit a large variance in the elements possibly due to pre-, syn- and/or post-eruptive processes.

Using this  $\mu$ -XRF scanning approach has not enabled clear geochemical separation between the Okaia and Tahuna tephra, nor separation of the Hauparu from the Maketu tephra (Fig. 8A). This further highlights the need for more elemental data points from each of the tephra layers, particularly the thinner layers (Fig. 2) to be able to better define mean count values of the elements, their variance, and hence, delineate possible outliers. In addition to acquiring more elemental data points during the scans, future work requires investigation of a greater range of elements, especially minor and trace elements<sup>2</sup>, which could achieve a clearer geochemical separation of the visually-distinct tephra.

#### Post-KOT Rhyolite Tephra

Scatterplots of Si vs. K, Ca vs. K, Fe vs. Si, Mn vs. Si, Ti vs. Cl, and Y vs. Cr for post-KOT rhyolitic tephra layers shown in Fig. 8B highlight the ease of differentiation of the Tuhua tephra from all others examined here. The thicker Rotoma and Rotorua layers can also be separated clearly despite an abundance of outliers, especially in the more common EPMA-based geochemical bivariate plots used commonly in tephrochronology (e.g.,  $\text{SiO}_2$  vs.  $\text{K}_2\text{O}$ ,  $\text{CaO}$  vs.  $\text{K}_2\text{O}$ ,  $\text{Fe}_2\text{O}_3$  vs.  $\text{SiO}_2$ ; Shane, 2000). The nature of these outliers is unclear but more precise Ca and Si  $\mu$ -XRF elemental data and potentially fewer outliers could be achieved on the Itrax  $\mu$ -XRF core scanner using the Cr-tube as it has lower detection limits for light elements. The minor elements contribute to separation of the post-KOT tephra layers with fewer outliers evident in Mn vs. Si, Ti vs. Cl and Y vs. Cr bivariate plots (Fig. 8B). The Opepe and Waiohau tephra do not plot as clearly defined clusters although the Opepe tephra data points define a zone where most of its elemental data points lie.

*Figure 8 about here, landscape over full page*

#### 5 Conclusions

This study demonstrates the potential of rapid and non-destructive  $\mu$ -XRF core scanning for separating rhyolitic tephra layers sourced from different volcanic centres, and sometimes different eruptives from the same centre using elemental composition. The ability to use compositional

---

<sup>2</sup> Following definition by glass shard geochemistry: major elements expressed as oxides are usually defined as >1 wt %, minor element oxides as 0.1 to 1 wt %, and trace elements as <0.1 wt % or <1000 parts per million (ppm) of the element (Lowe et al., 2017).

analyses derived from  $\mu$ -XRF core scanning as an aid to tephrochronology is abetted by the organic-rich lacustrine sediment interbedded with the tephra infilling the Auckland maar lakes that allow clear differentiation of the rhyolite tephra. This was able to be achieved despite the  $\mu$ -XRF core scanner measurements being generated using a Mo tube so that the light element data (Al, Ca) were of lower precision than if a Cr tube was used. These elements are typically useful in conventional tephra fingerprinting using major oxide data derived from electron microprobe analysis. Analyses of minor and trace elements can be useful in tephra fingerprinting (e.g. Pearce et al., 2007; Davies et al., 2012; Wastegård et al., 2013; Lowe et al., 2017), which are easily and quickly obtained by  $\mu$ -XRF core scanning during the same analysis as major elements are acquired. Consequently, future studies should evaluate the full potential of the  $\mu$ -XRF scanning technique for tephra fingerprinting by varying the scanning settings and elements used. In particular, exposure time per measurement interval and scanning settings need to be adjusted in order for the elemental counts to exceed “0” where relevant, in order to avoid discarding many minor and trace elements that may be of significance. Only then can the whole range of geochemical variability between tephra layers be captured and utilised. Similarly, obtaining Al and Ca counts as high as possible might need to be the focus when choosing the X-ray tube (favouring the Cr-tube for the light elements) and adjusting scanning settings (kV, mA) and exposure time accordingly.

This study also shows that many factors, such as current (mA), voltage (kV) and exposure time influence scanning results in a non-linear manner. Their influence has not yet been quantified and we propose to avoid these complications by following a standard protocol for tephra characterisation. Experimental scans of tephra layers to be undertaken in the future should determine ideal current, voltage and exposure time to enable robust data comparison and application of multivariate statistics.

An additional complication for robust tephra  $\mu$ -XRF based fingerprinting arises from the difference between different generation detector systems and related settings in the Itrax  $\mu$ -XRF core scanners used in this study. Despite normalisation of elemental count data, significant differences between data sets from the same maar cores and tephra layers scanned by different core scanners remained. To avoid this complication in the future, we propose to conduct all further tephra  $\mu$ -XRF scans for New Zealand tephra layers on the same Itrax core scanner following a standard protocol.

The results of the present study suggest that only one or two bivariate scatterplots (e.g., Ca vs. K, Rb vs. Sr, Y vs. Cr; Fig. 8) of  $\mu$ -XRF core scanning data may be enough to fingerprint one or more rhyolite tephra layers. However, thin tephra layers, such as the Tahuna, Hauparu, Okaia, Okareka, Waiohau,

Opepe and Mamaku examined in the present study need to be investigated with repetitive  $\mu$ -XRF scans to obtain greater data density for the statistical approaches used.

Using these protocols, it is possible to establish a database of many  $\mu$ -XRF scanning results from tephra layers already identified using EPMA-based approaches which can be used as the input to semi-automated machine learning algorithms to reliably identify rhyolitic tephra and thereby decrease the time involved in tephra fingerprinting for tephrochronology in a non-destructive manner. To be able to utilize this method of  $\mu$ -XRF core scanning-based tephra fingerprinting to its full potential, the approach will need to be extended to basaltic and andesitic tephra layers that are commonly encountered in the AVF maar lakes sediment cores. Subsequently, tephrochronologists working in other regions of the globe in which tephra layers of sufficient thickness are found in lake sediments and peat may be able to use this approach. New Zealand is highly suitable to develop a  $\mu$ -XRF method for geochemically fingerprinting rhyolitic tephra layers due to the rhyolitic eruptives from several volcanoes and volcanic centres being significantly different in their geochemical composition. On the other hand, many volcanic systems in the world have erupted tephras of similar composition throughout their history (e.g., southern America, Iceland, Anatolia). These tephra may not be identifiable by  $\mu$ -XRF scanning. As  $\mu$ -XRF data from sediment cores are routinely acquired in a rapid, semi-automated and non-destructive manner, the  $\mu$ -XRF based geochemical composition of these tephra layers can easily be studied and compared for differences. An increase in XRF exposure time and modern detector technology may provide crucial trace elemental data, which may highlight differences between these tephra layers. Detailed scans and comparison to the volcanic source are necessary on a regional scale if implementation of this  $\mu$ -XRF based approach is sought outside of New Zealand. In addition, studies need to be undertaken in sediment cores from marine and minerogenic terrestrial depositional environments to widen the possible applicability of this promising approach.

Established techniques such as EPMA and LA-ICP-MS acquire data from single grains/glass shards whereas the  $\mu$ -XRF scanner obtains data from the bulk of the tephra layer. In both techniques measurements on 10 - 20 grains (EPMA, LA-ICP-MS) and over numerous downcore positions of the tephra layer ( $\mu$ -XRF) are obtained to capture subtle differences throughout a layer. Careful comparison between EPMA-derived composition of glass shards and corresponding  $\mu$ -XRF-based composition of the bulk tephra layer are to be conducted in the future since we have now demonstrated the general applicability of  $\mu$ -XRF data to tephrochronology. Large compositional heterogeneity in tephra layers due to pre- and syn-eruptive processes (Shane et al., 2008) rely on EPMA or LA-ICP-MS measurements on separate grains or glass shards in EPMA or LA-ICP-MS. As a result of the small step size of the  $\mu$ -XRF core scanner, this technique may be employed to study

subtle differences in the chemical composition and grain size of tephra layers along the core axis, i.e., during its eruptive and/or depositional history.

Classical EPMA- and LA-ICP-MS-based chemical fingerprinting of tephra are supported by their stratigraphic order, physical properties such as thickness and colour, and independent ages to enable them to be correlated (Lowe et al., 2017). The same indicators must not be ignored in  $\mu$ -XRF scanning based fingerprinting of tephra layers.

The speed of elemental scanning and wide range of elements detected in tephra layers makes the  $\mu$ -XRF scanning approach a possible future tool for refining tephra correlation work in which traditional methods have failed to establish unambiguous correlations between given layers. This is partly the case with strong inhomogeneity in the 30+ basaltic tephra layers encountered in the AVF (Hopkins et al., 2015; 2017). Volcanic hazard assessment for Auckland city with >1.5 million inhabitants and infrastructure of national importance largely depends on correct tephra correlation and age estimates of tephra layers produced by eruptions from the AVF volcanoes.

#### Acknowledgements

We thank two anonymous reviewers for their helpful comments, which have strongly improved an earlier version of this manuscript. LP thanks the School of Environment, University of Auckland for supporting her participation in the Itrax Advanced Operator Training Course by Cox Analytical Systems in Stockholm, Sweden. LP expresses her gratitude to Cox Analytical Systems, in particular to Per Engström, for fundamental training and on-going support with data processing. LP acknowledges financial support from the University of Auckland Doctoral Scholarship and the Australian Institute for Nuclear Science and Engineering Post-Graduate Research Award.

#### Funding sources

Itrax scans at the University of Auckland have been funded by RSNZ Marsden Fund Contract UOA1415 and AINSE Ltd Award No. ALNGRA11064 (at ANSTO). Itrax scans at the Aberystwyth University were funded by Marsden contract UOA0415.

#### Conflict of Interest

The authors report no conflict of interest.

#### References

Aitchison, J., 1986. The statistical analysis of compositional data. Chapman and Hall, London; New York.

- 475 Augustinus, P., 2007. NZ-Maars: Extracting high resolution paleoclimate records from maar crater  
476 lakes, Auckland, New Zealand. *PAGES News* 15, 18–20.
- 477 Augustinus, P., Reid, M., Andersson, S., Deng, Y., Horrocks, M., 2006. Biological and geochemical  
478 record of anthropogenic impacts in recent sediments from Lake Pupuke, Auckland City, New  
479 Zealand. *Journal of Paleolimnology* 35, 789–805. doi:10.1007/s10933-005-5306-8
- 480 Augustinus, P., Bleakley, N., Deng, Y., Shane, P., Cochran, U., 2008. Rapid change in early Holocene  
481 environments inferred from Lake Pupuke, Auckland City, New Zealand. *Journal of Quaternary*  
482 *Science* 23, 435–447. doi:10.1002/jqs.1153
- 483 Augustinus, P., D’Costa, D., Deng, Y., Hagg, J., Shane, P., 2011. A multi-proxy record of changing  
484 environments from ca. 30000 to 9000 cal. a BP: Onepoto maar palaeolake, Auckland, New  
485 Zealand. *Journal of Quaternary Science* 26, 389–401. doi:10.1002/jqs.1463
- 486 Balascio, N.L., Francus, P., Bradley, R.S., Schupack, B.B., Miller, G.H., Kvisvik, B.C., Bakke, J.,  
487 Thordarson, T., 2015. Investigating the Use of Scanning X-Ray Fluorescence to Locate  
488 Cryptotephra in Minerogenic Lacustrine Sediment: Experimental Results. In: Croudace, I.W.,  
489 Rothwell, R.G. (Eds.), *Micro-XRF Studies of Sediment Cores: Applications of a Non-Destructive*  
490 *Tool for the Environmental Sciences*. Springer Science+Business Media, Dordrecht, pp. 305–  
491 324.
- 492 Cas, R.A.F., Wright, J. V., 1988. *Volcanic Successions Modern and Ancient - A geological approach to*  
493 *processes, products and successions*, 1st ed. Chapman and Hall, London.
- 494 Cronin, S.J., Neall, V.E., Stewart, R.B., Palmer, A.S., 1996. A multiple-parameter approach to andesitic  
495 tephra correlation, Ruapehu volcano, New Zealand. *Journal of Volcanology and Geothermal*  
496 *Research* 72, 199–215. doi:10.1016/0377-0273(96)00008-X
- 497 Croudace, I.W., Rothwell, R.G., 2010. Micro-XRF sediment core scanners: important new tools for  
498 the environmental and earth sciences. *Spectroscopy Europe* 22, 6–13.
- 499 Croudace, I.W., Rindby, A., Rothwell, R.G., 2006. ITRAX: description and evaluation of a new multi-  
500 function X-ray core scanner. Geological Society, London, Special Publications 267, 51–63.  
501 doi:10.1144/GSL.SP.2006.267.01.04
- 502 Cuven, S., Francus, P., Cremer, J.F., 2007. Protocoles d’utilisation et essais de calibration du scanner  
503 de micro-fluorescence X de type “Itrax Core Scanner,” Inrs-Ete.
- 504 Danišík, M., Shane, P., Schmitt, A.K., Hogg, A., Santos, G.M., Storm, S., Evans, N.J., Keith Fifield, L.,  
505 Lindsay, J.M., 2012. Re-anchoring the late Pleistocene tephrochronology of New Zealand based



- 506 on concordant radiocarbon ages and combined  $^{238}\text{U}/^{230}\text{Th}$  disequilibrium and (U-Th)/He  
 507 zircon ages. *Earth and Planetary Science Letters* 349–350, 240–250.  
 508 doi:10.1016/j.epsl.2012.06.041
- 509 Davies, S.J., Lamb, H.F., Roberts, S.J., 2015. Micro-XRF Core Scanning in Palaeolimnology: Recent  
 510 Developments. In: Croudace, I.W., Rothwell, R.G. (Eds.), *Micro-XRF Studies of Sediment Cores*  
 511 *Applications of a Non-Destructive Tool for the Environmental Sciences*. Springer, Dordrecht, p.  
 512 656.
- 513 Davies, S.M., Abbott, P.M., Pearce, N.J.G., Wastegård, S., Blockley, S.P.E., 2012. Integrating the  
 514 INTIMATE records using tephrochronology: Rising to the challenge. *Quaternary Science*  
 515 *Reviews* 36, 11–27. doi:10.1016/j.quascirev.2011.04.005
- 516 Dugmore, A.J., Newton, A.J., 2012. Isochrons and beyond: maximising the use of tephrochronology  
 517 in geomorphology. *Jökull* 62, 39–52.
- 518 Feng, C., Wang, H., Lu, N., Chen, T., He, H., Lu, Y., Tu, X.M., 2014. Log-transformation and its  
 519 implications for data analysis. *Shanghai archives of psychiatry* 26, 105–9.  
 520 doi:10.3969/j.issn.1002-0829.2014.02.009
- 521 Hopkins, J.L., Millet, M.A., Timm, C., Wilson, C.J.N., Leonard, G.S., Palin, J.M., Neil, H., 2015. Tools  
 522 and techniques for developing tephra stratigraphies in lake cores: A case study from the  
 523 basaltic Auckland Volcanic Field, New Zealand. *Quaternary Science Reviews* 123, 58–75.  
 524 doi:10.1016/j.quascirev.2015.06.014
- 525 Hopkins, J.L., Wilson, C.J.N., Millet, M.A., Leonard, G.S., Timm, C., McGee, L.E., Smith, I.E.M., Smith,  
 526 E.G.C., 2017. Multi-criteria correlation of tephra deposits to source centres applied in the  
 527 Auckland Volcanic Field, New Zealand. *Bulletin of Volcanology* 79. doi:10.1007/s00445-017-  
 528 1131-y
- 529 Kylander, M.E., Lind, E.M., Wastegard, S., Lowemark, L., 2012. Recommendations for using XRF core  
 530 scanning as a tool in tephrochronology. *The Holocene* 22, 371–375.  
 531 doi:10.1177/0959683611423688
- 532 Lane, C.S., Lowe, D.J., Blockley, S.P.E., Suzuki, T., Smith, V.C., 2017. Advancing tephrochronology as a  
 533 global dating tool: Applications in volcanology, archaeology, and palaeoclimatic research.  
 534 *Quaternary Geochronology* 40, 1–7. doi:10.1016/j.quageo.2017.04.003
- 535 Leonard, G.S., Calvert, A.T., Hopkins, J.L., Wilson, C.J.N., Smid, E.R., Lindsay, J.M., Champion, D.E.,  
 536 2017. High-precision  $^{40}\text{Ar}/^{39}\text{Ar}$  dating of Quaternary basalts from Auckland Volcanic Field,



- 537 New Zealand, with implications for eruption rates and paleomagnetic correlations. *Journal of*  
 538 *Volcanology and Geothermal Research* 343, 60–74. doi:10.1016/j.jvolgeores.2017.05.033
- 539 Lindsay, J., Leonard, G., Smid, E., Hayward, B., 2011. Age of the Auckland Volcanic Field: a review of  
 540 existing data. *New Zealand Journal of Geology and Geophysics* 54, 379–401.  
 541 doi:10.1080/00288306.2011.595805
- 542 Lowe, D.J., 2011. Tephrochronology and its application: A review. *Quaternary Geochronology* 6,  
 543 107–153. doi:10.1016/j.quageo.2010.08.003
- 544 Lowe, D.J., Shane, P.A.R., Alloway, B. V., Newnham, R.M., 2008. Fingerprints and age models for  
 545 widespread New Zealand tephra marker beds erupted since 30,000 years ago: a framework for  
 546 NZ-INTIMATE. *Quaternary Science Reviews* 27, 95–126. doi:10.1016/j.quascirev.2007.01.013
- 547 Lowe, D.J., Blaauw, M., Hogg, A.G., Newnham, R.M., 2013. Ages of 24 widespread tephras erupted  
 548 since 30,000 years ago in New Zealand, with re-evaluation of the timing and palaeoclimatic  
 549 implications of the Lateglacial cool episode recorded at Kaipo bog. *Quaternary Science Reviews*  
 550 74, 170–194. doi:10.1016/j.quascirev.2012.11.022
- 551 Lowe, D.J., Pearce, N.J.G., Jorgensen, M.A., Kuehn, S.C., Tryon, C.A., Hayward, C.L., 2017. Correlating  
 552 tephras and cryptotephras using glass compositional analyses and numerical and statistical  
 553 methods: Review and evaluation. *Quaternary Science Reviews* 175, 1–44.  
 554 doi:10.1016/j.quascirev.2017.08.003
- 555 Löwemark, L., Chen, H.F., Yang, T.N., Kylander, M., Yu, E.F., Hsu, Y.W., Lee, T.Q., Song, S.R., Jarvis, S.,  
 556 2011. Normalizing XRF-scanner data: A cautionary note on the interpretation of high-resolution  
 557 records from organic-rich lakes. *Journal of Asian Earth Sciences* 40, 1250–1256.  
 558 doi:10.1016/j.jseaes.2010.06.002
- 559 Martin-Puertas, C., Tjallingii, R., Bloemsma, M., Brauer, A., 2017. Varved sediment responses to early  
 560 Holocene climate and environmental changes in Lake Meerfelder Maar (Germany) obtained  
 561 from multivariate analyses of micro X-ray fluorescence core scanning data. *Journal of*  
 562 *Quaternary Science* 32, 427–436. doi:10.1002/jqs.2935
- 563 Molloy, C., Shane, P., Augustinus, P., 2009. Eruption recurrence rates in a basaltic volcanic field  
 564 based on tephrallayers in maar sediments: Implications for hazards in the Auckland volcanic  
 565 field. *Bulletin of the Geological Society of America* 121, 1666–1677. doi:10.1130/B26447.1
- 566 Newnham, R., Lowe, D.J., Gehrels, M., Augustinus, P., 2018. Two-step human–environmental impact  
 567 history for northern New Zealand linked to late-Holocene climate change. *Holocene*.

- 568 doi:10.1177/0959683618761545
- 569 Nilsson, A., Muscheler, R., Snowball, I., Aldahan, A., Possnert, G., Augustinus, P., Atkin, D., Stephens,  
570 T., 2011. Multi-proxy identification of the Laschamp geomagnetic field excursion in Lake  
571 Pupuke, New Zealand. *Earth and Planetary Science Letters* 311, 155–164.  
572 doi:10.1016/j.epsl.2011.08.050
- 573 Pearce, N.J.G., Denton, J.S., Perkins, W.T., Westgate, J.A., Alloway, B. V., 2007. Correlation and  
574 characterisation of individual glass shards from tephra deposits using trace element laser  
575 ablation ICP-MS analyses: current status and future potential. *Journal of Quaternary Science*  
576 22, 721–736.
- 577 Pearce, N.J.G., Bendall, C.A., Westgate, J.A., 2008. Comment on “Some numerical considerations in  
578 the geochemical analysis of distal microtephra” by A.M. Pollard, S.P.E. Blockley and C.S. Lane.  
579 *Applied Geochemistry* 23, 1353–1364. doi:10.1016/j.apgeochem.2008.01.002
- 580 Pepper, A.C., Shulmeister, J., Nobes, D.C., Augustinus, P.A., 2004. Possible ENSO signals prior to the  
581 Last Glacial Maximum, during the last deglaciation and the early Holocene, from New Zealand.  
582 *Geophysical Research Letters* 31, 1–4. doi:10.1029/2004GL020236
- 583 Rothwell, R.G., Croudace, I.W., 2015. Twenty Years of XRF Core Scanning Marine Sediments: What  
584 Do Geochemical Proxies Tell Us? In: Croudace, I.W., Rothwell, R.G. (Eds.), *Micro-XRF Studies of*  
585 *Sediment Cores Applications of a Non-Destructive Tool for the Environmental Sciences*.  
586 Springer, Dordrecht, p. 656.
- 587 Shane, P., 2000. Tephrochronology: A New Zealand case study, *Earth Science Reviews*.  
588 doi:10.1016/S0012-8252(99)00058-6
- 589 Shane, P., 2005. Towards a comprehensive distal andesitic tephrostratigraphic framework for New  
590 Zealand based on eruptions from Egmont volcano. *Journal of Quaternary Science* 20, 45–57.  
591 doi:10.1002/jqs.897
- 592 Shane, P., Smith, I., 2000. Geochemical fingerprinting of basaltic tephra deposits in the Auckland  
593 Volcanic Field. *New Zealand Journal of Geology and Geophysics* 43, 569–577.  
594 doi:10.1080/00288306.2000.9514909
- 595 Shane, P., Nairn, I.A., Martin, S.B., Smith, V.C., 2008. Compositional heterogeneity in tephra deposits  
596 resulting from the eruption of multiple magma bodies: Implications for tephrochronology.  
597 *Quaternary International* 178, 44–53. doi:10.1016/j.quaint.2006.11.014
- 598 Shane, P.A.R., Froggatt, P.C., 1994. Discriminant Function Analysis of Glass Chemistry of New Zealand

- 599 and North American Tephra Deposits. *Quaternary Research* 41, 70–81.  
 600 doi:10.1006/qres.1994.1008
- 601 Smith, I.E.M., 1989. New Zealand Intraplate Volcanism: North Island. In: Johnson, R.W. (Ed.),  
 602 Intraplate Volcanism in Eastern Australia and New Zealand. Cambridge University Press,  
 603 Cambridge, UK, pp. 157–188.
- 604 Stephens, T., Atkin, D., Cochran, U., Augustinus, P., Reid, M., Lorrey, A., Shane, P., Street-Perrott, A.,  
 605 2012. A diatom-inferred record of reduced effective precipitation during the Last Glacial  
 606 Coldest Phase (28.8–18.0 cal kyr BP) and increasing Holocene seasonality at Lake Pupuke,  
 607 Auckland, New Zealand. *Journal of Paleolimnology* 48, 801–817. doi:10.1007/s10933-012-9645-  
 608 y
- 609 Stokes, S., Lowe, D.J., 1988. Discriminant function analysis of late Quaternary tephra from five  
 610 volcanoes in New Zealand using glass shard major element chemistry. *Quaternary Research* 30,  
 611 270–283. doi:10.1016/0033-5894(88)90003-8
- 612 Stokes, S., Lowe, D.J., Froggatt, P.C., 1992. Discriminant function analysis and correlation of Late  
 613 Quaternary rhyolitic tephra deposits from Taupo and Okataina volcanoes, New Zealand, using  
 614 glass shard major element composition. *Quaternary International* 13–14, 103–117.  
 615 doi:10.1016/1040-6182(92)90016-U
- 616 Striewski, B., Shulmeister, J., Augustinus, P.C., Soderholm, J., 2013. Late Holocene climate variability  
 617 from Lake Pupuke maar, Auckland, New Zealand. *Quaternary Science Reviews* 77, 46–54.  
 618 doi:10.1016/j.quascirev.2013.07.003
- 619 Thomson, J., Croudace, I.W., Rothwell, R.G., 2006. A geochemical application of the ITRAX scanner to  
 620 a sediment core containing eastern Mediterranean sapropel units. Geological Society, London,  
 621 Special Publications 267, 65–77. doi:10.1144/gsl.sp.2006.267.01.05
- 622 Wastegård, S., Veres, D., Kliem, P., Hahn, A., Ohlendorf, C., Zolitschka, B., 2013. Towards a late  
 623 Quaternary tephrochronological framework for the southernmost part of South America - the  
 624 Laguna Potrok Aike tephra record. *Quaternary Science Reviews* 71, 81–90.  
 625 doi:10.1016/j.quascirev.2012.10.019
- 626 Weltje, G.J., Tjallingii, R., 2008. Calibration of XRF core scanners for quantitative geochemical logging  
 627 of sediment cores: Theory and application. *Earth and Planetary Science Letters* 274, 423–438.  
 628 doi:10.1016/j.epsl.2008.07.054
- 629 Weltje, G.J., Bloemsa, M.R., Tjallingii, R., Heslop, D., Croudace, I.W., 2015. Prediction of

Geochemical Composition from XRF Core Scanner Data : A New Multivariate Approach

Including Automatic Selection of Calibration Samples and Quantification of Uncertainties. In:

Croudace, I.W., Rothwell, R.G. (Eds.), Micro-XRF Studies of Sediment Cores: Applications of a

Non-Destructive Tool for the Environmental Sciences. Springer Science+Business Media,

Dordrecht, pp. 507–534. doi:10.1007/978-94-017-9849-5

Winter, J.D., 2001. An Introduction to Igneous and Metamorphic Petrology. Prentice Hall Inc., Upper  
Saddle River, New Jersey.

Zawalna-Geer, A., Lindsay, J.M., Davies, S., Augustinus, P., Davies, S., 2016. Extracting a primary  
Holocene cryptoptephra record from Pupuke maar sediments, Auckland, New Zealand. Journal  
of Quaternary Science 31, 442–457. doi:10.1002/jqs.2866

Zelterman, D., 2015. Applied Multivariate Statistics with R. Springer, Heidelberg, New York,  
Dordrecht, London. doi:10.1007/978-3-319-14093-3

Figure 1: Auckland Volcanic Field (left) with maar craters of this study highlighted in red and its position in New Zealand's North Island (right) in relation to the volcanic sources of the tephra layers found in the Auckland maars and wider New Zealand area: Tuhua (TUV, peralkaline rhyolitic), Taupo (TV, rhyolitic) and Okataina (OV, rhyolitic), Egmont (Eg volcano, andesitic), Tongariro (TgV, andesitic) and Auckland Volcanic Field (AVF, basaltic). VC: volcanic centre.

Figure 2: Variation of ten normalised elemental counts from  $\mu$ -XRF core scanning across (A) six pre-KOT layers and (B) seven post-KOT layers alongside their optical core images. Note the contrast in  $\mu$ -XRF data between enclosing sediment and rhyolite tephra layers.

Figure 3: Kernel density of normalised elemental counts of all 13 tephra layers analysed. Note how most elements approximate a log-normal distribution.

Figure 4: Kernel density of  $K_{\text{norm}}$  (up),  $Ca_{\text{norm}}$  (center), and  $Sr_{\text{norm}}$  (bottom) of all tephra  $\mu$ -XRF core scanning data. Coloured lines differentiate between pre-identified tephra layers. Line pattern differentiates between Itrax lab locations of respective  $\mu$ -XRF data. Note how, for example, the Tahuna tephra shows very different peaks depending on the scanning location whereas the  $Sr_{\text{norm}}$  peaks of the Rotoma tephra from UOA and UA almost overlap.

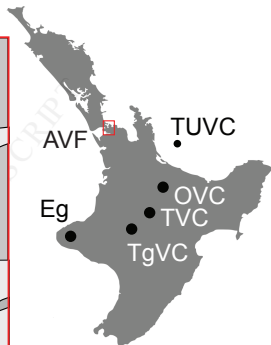
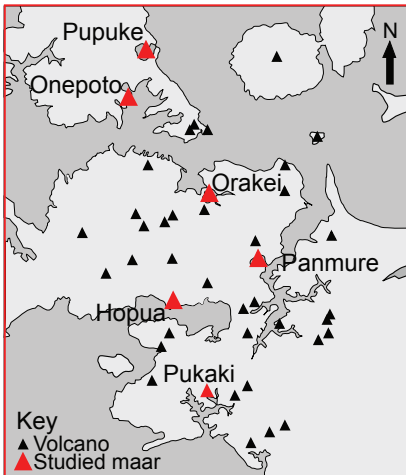
Figure 5: Principal component analysis of (A) log-ratio-transformed  $\mu$ -XRF scanning results from the Onepoto core (pre-KOT) measured at ANSTO; (B) log-ratio-transformed  $\mu$ -XRF scanning results from the Hopua core (post-KOT) measured at the University of Auckland; (C) and non-transformed  $\mu$ -XRF scanning results as in B. Note how the log-transformed data plots in clusters with a larger spread of the datapoints than not transformed data. The log-transformed data also does not capture a cluster of the Tuhua tephra whereas not transformed data results in narrower clusters and captures clearly separated clusters for the Tuhua and Rotoma tephra.

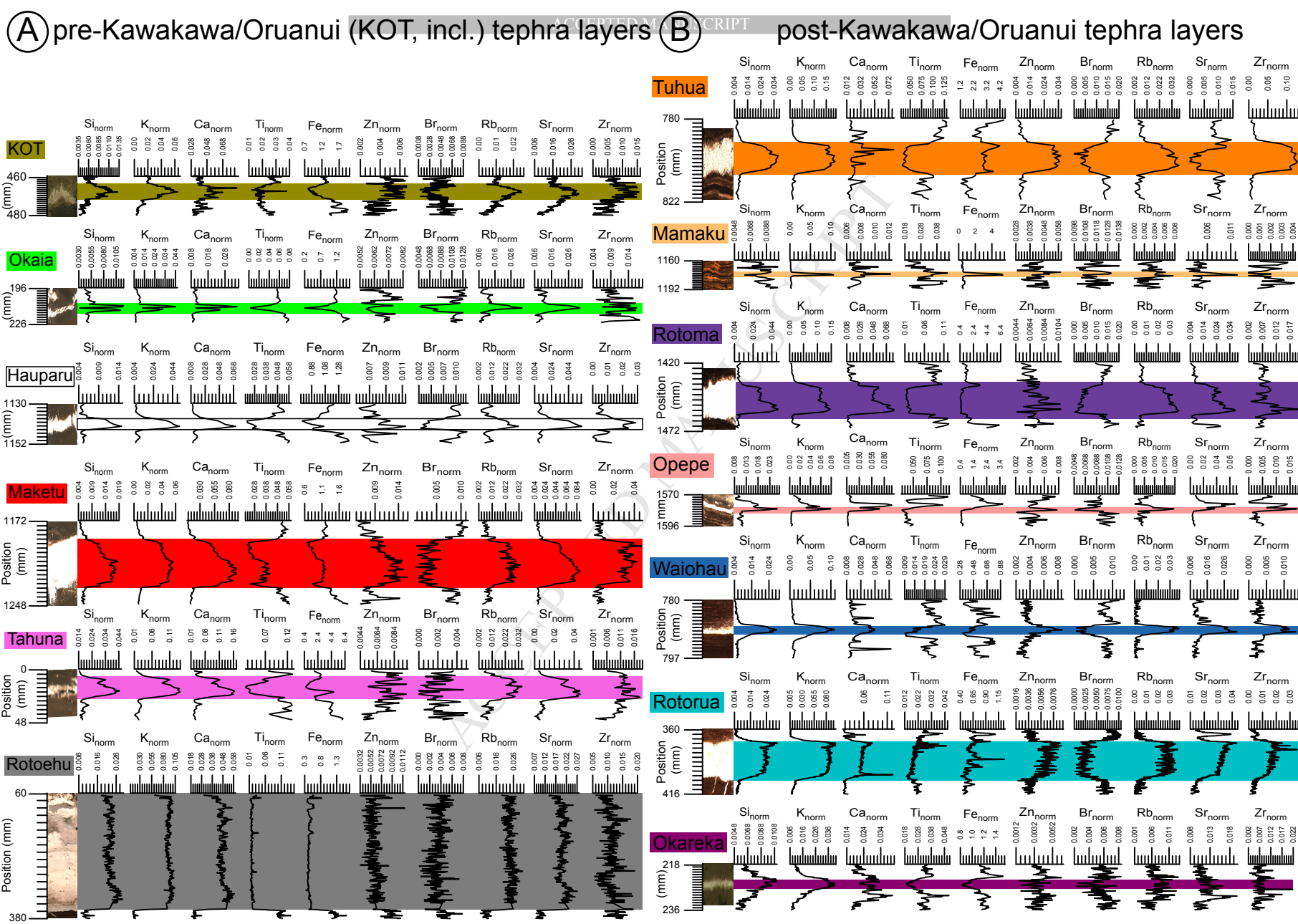
Figure 6: Principal component analysis of (A) log-ratio-transformed  $\mu$ -XRF scanning results from the rhyolitic tephra layers in the Onepoto core (pre-KOT) measured at ANSTO; (B) log-ratio-transformed  $\mu$ -XRF scanning results from the rhyolitic tephra layers in the Hopua and Panmure cores (post-KOT) measured at UOA. Note how all thicker tephra layers with >50 data points (Rotoehu, Maketu, Rotorua, Rotoma, Tuhua) form clear clusters.

Figure 7: Linear discriminant analysis of (A) log-ratio-transformed  $\mu$ -XRF scanning results from the rhyolitic tephra layers in the Onepoto core (pre-KOT) measured at ANSTO; (B) log-ratio-transformed  $\mu$ -XRF scanning results from the rhyolitic tephra layers in the Hopua and Panmure cores (post-KOT) measured at the University of Auckland. Note that LD2 enables discrimination between the source

volcanic centres (TVC and OVC) in (A) and LD1 separates TU vs. TVC+OVC, whilst LD3 separates TVC vs. OVC+MI in (B). Black arrows mark the direction of relative enrichment of elements listed.

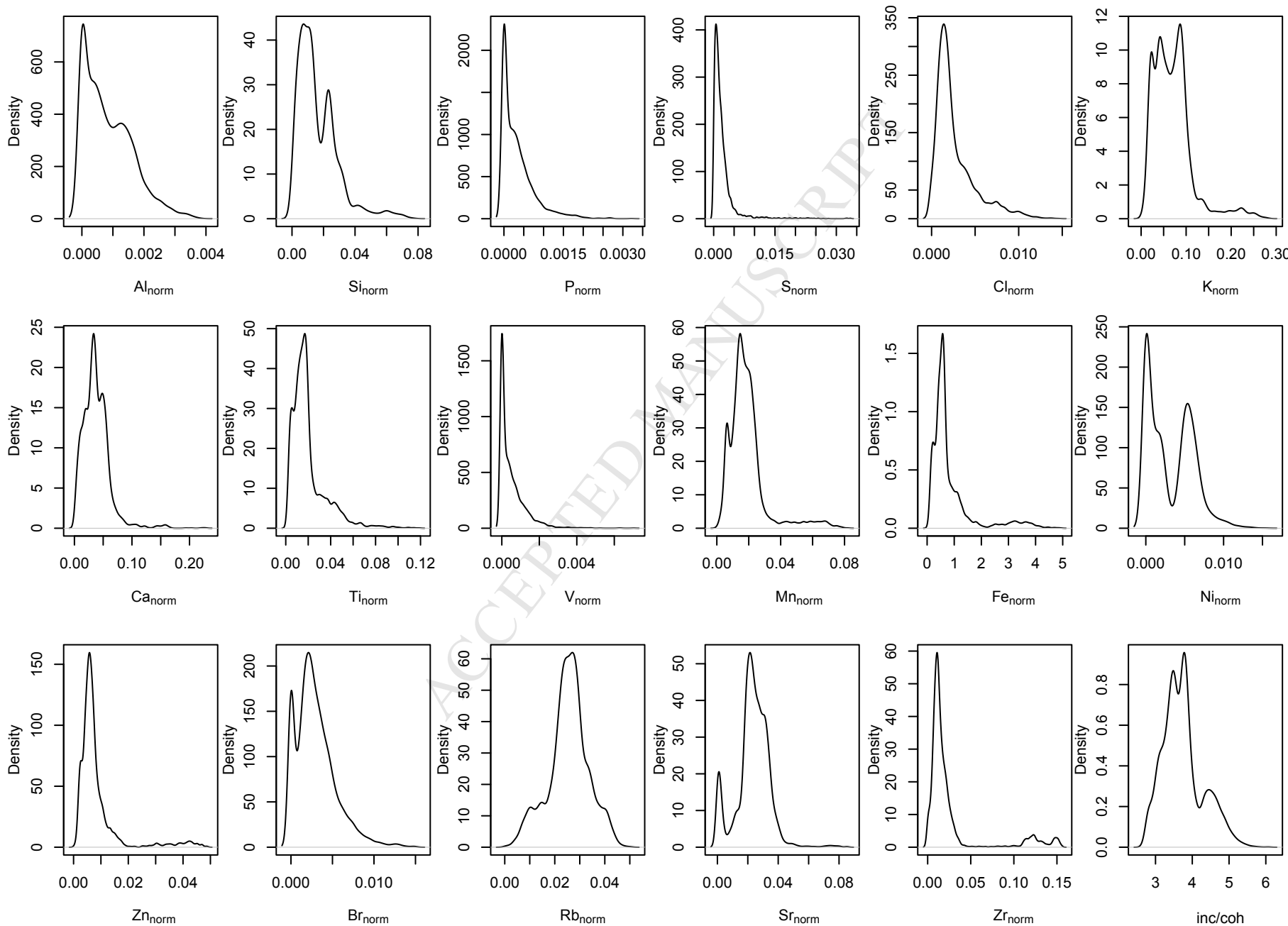
Figure 8: Bivariate scatter plots of six elemental ratios of (A) log-transformed  $\mu$ -XRF scanning results from the rhyolitic tephra layers in the Onepoto core (pre-KOT) measured at ANSTO; (B) log-transformed  $\mu$ -XRF scanning results from the rhyolitic tephra layers in the Hopua and Panmure cores (post-KOT) measured at the University of Auckland. Note how most plots allow for clear separation of the thicker tephra layers (Okaia, Maketu, Rotoehu in (A); Tuhua, Rotoma, Opepe and Rotorua tephra in (B)).

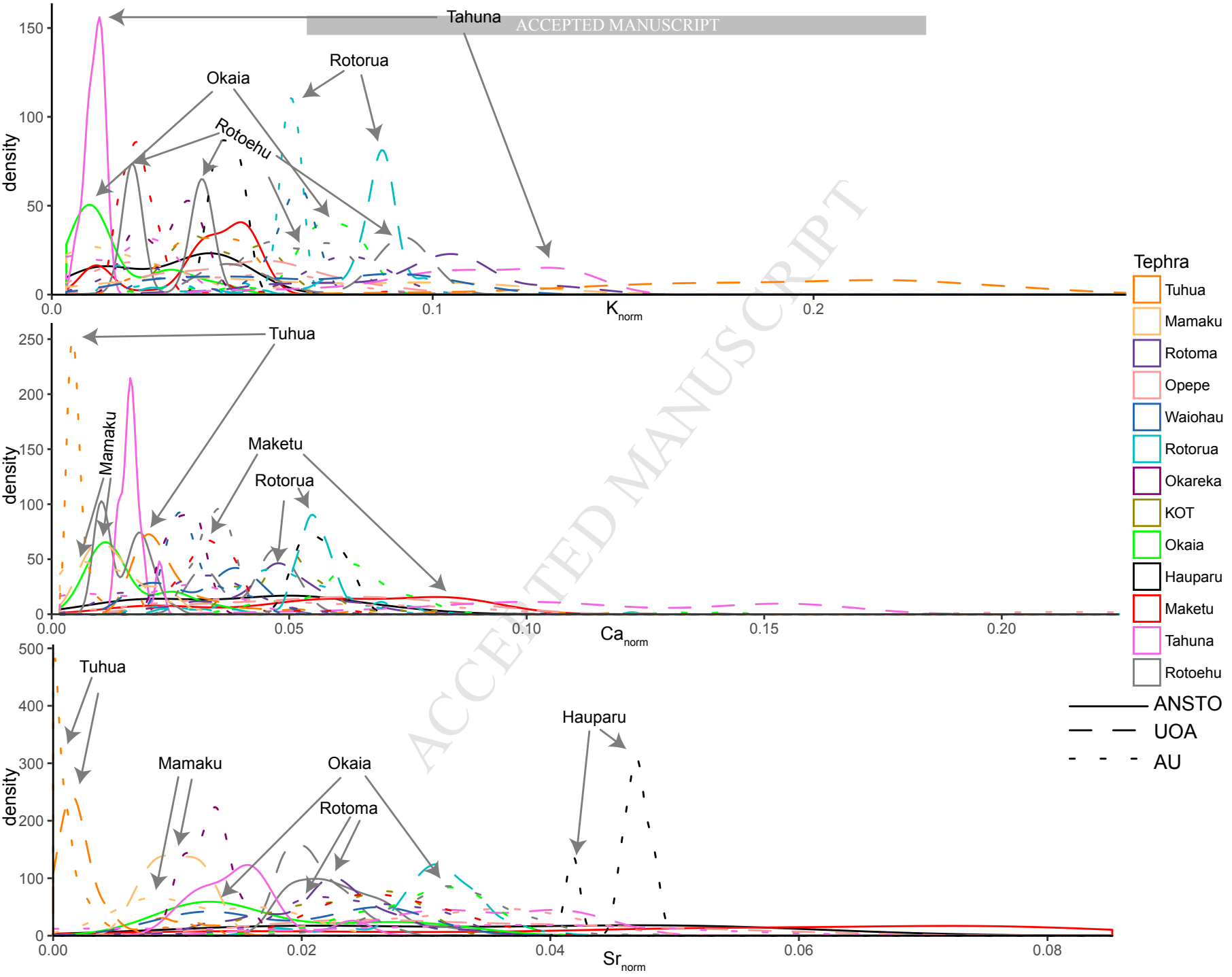






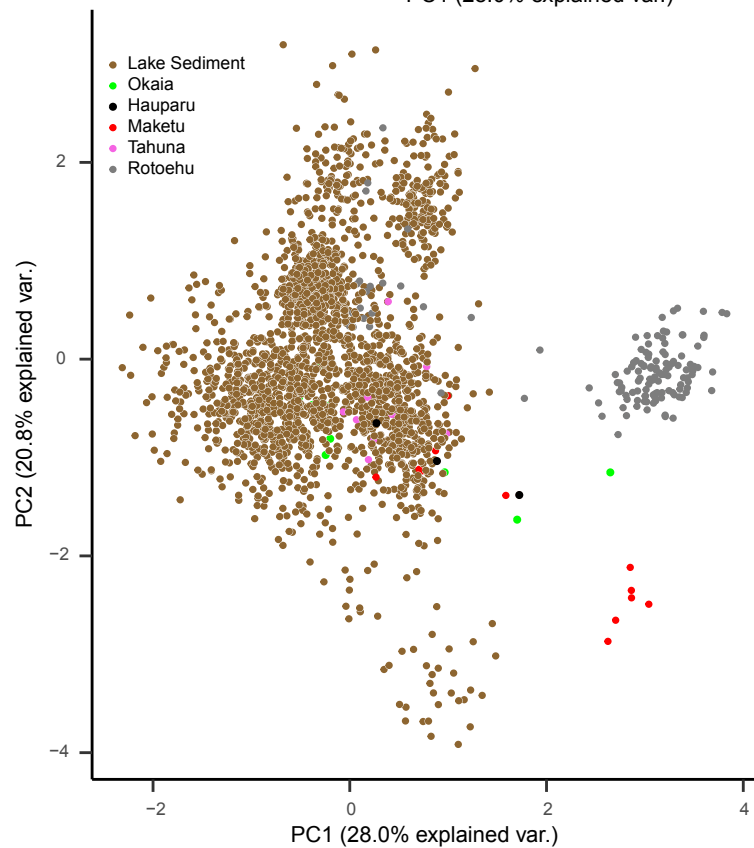
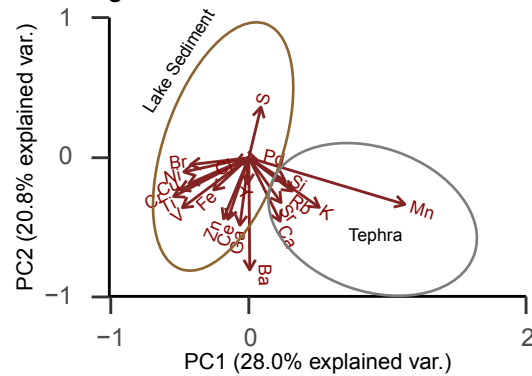
# Kernel density plots of elements X<sub>norm</sub> and inc/coh scattering ratio (all 13 tephra layers, all measurements, not transformed)





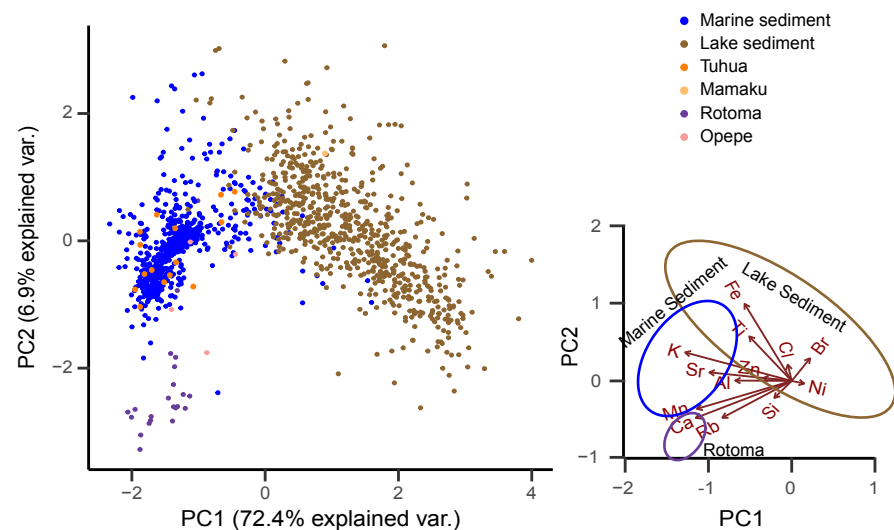
**(A)**

Onepoto (measured at ANSTO);  
pre-KOT; log-ratio transformed



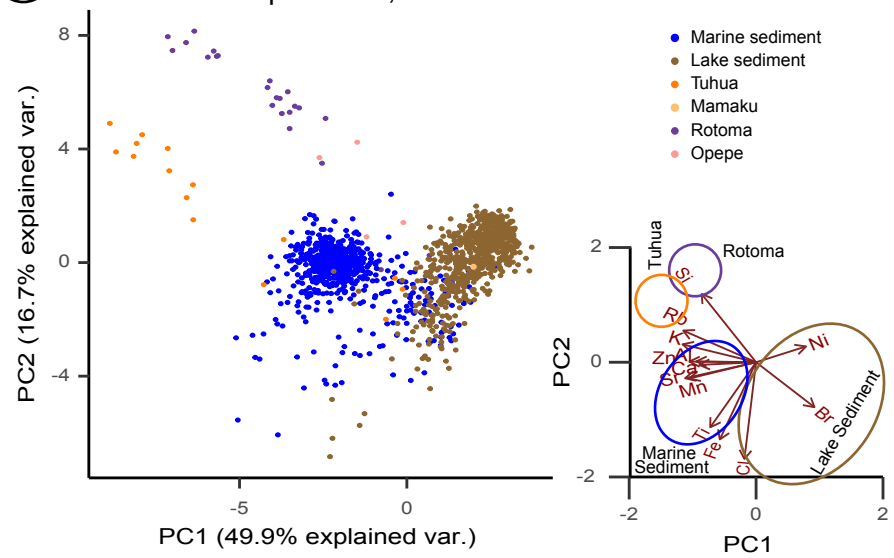
**(B)**

Hopua (measured at Auckland);  
post-KOT; log-ratio transformed

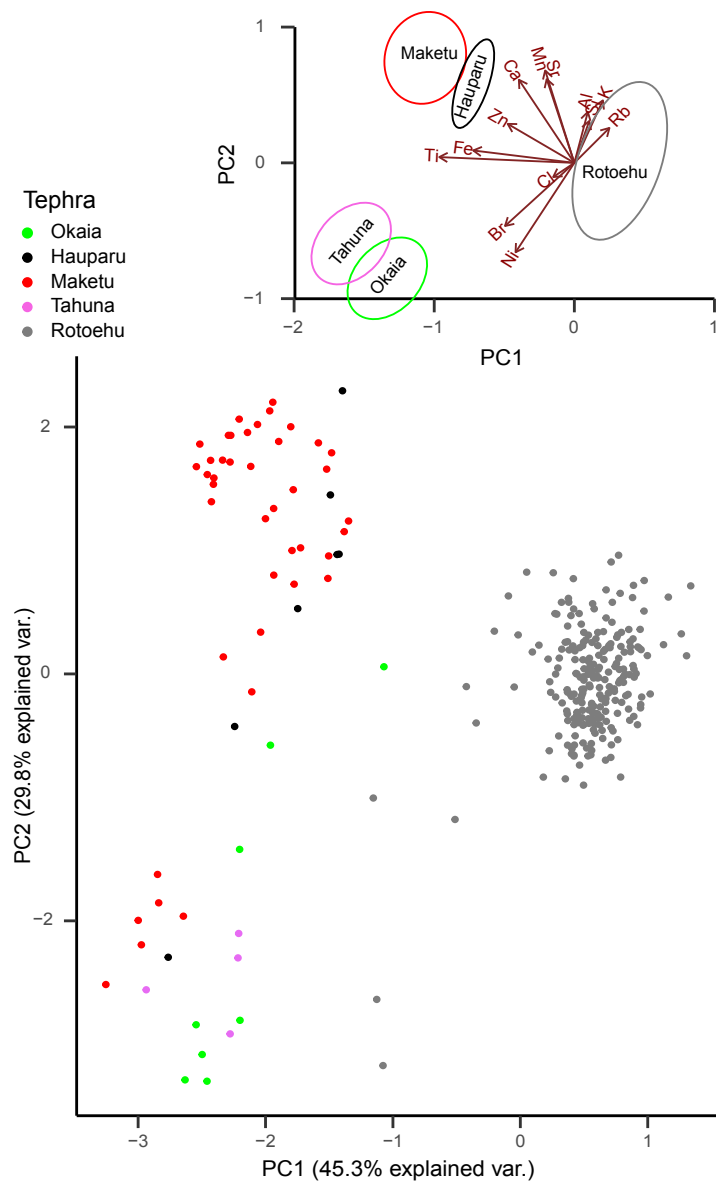


**(C)**

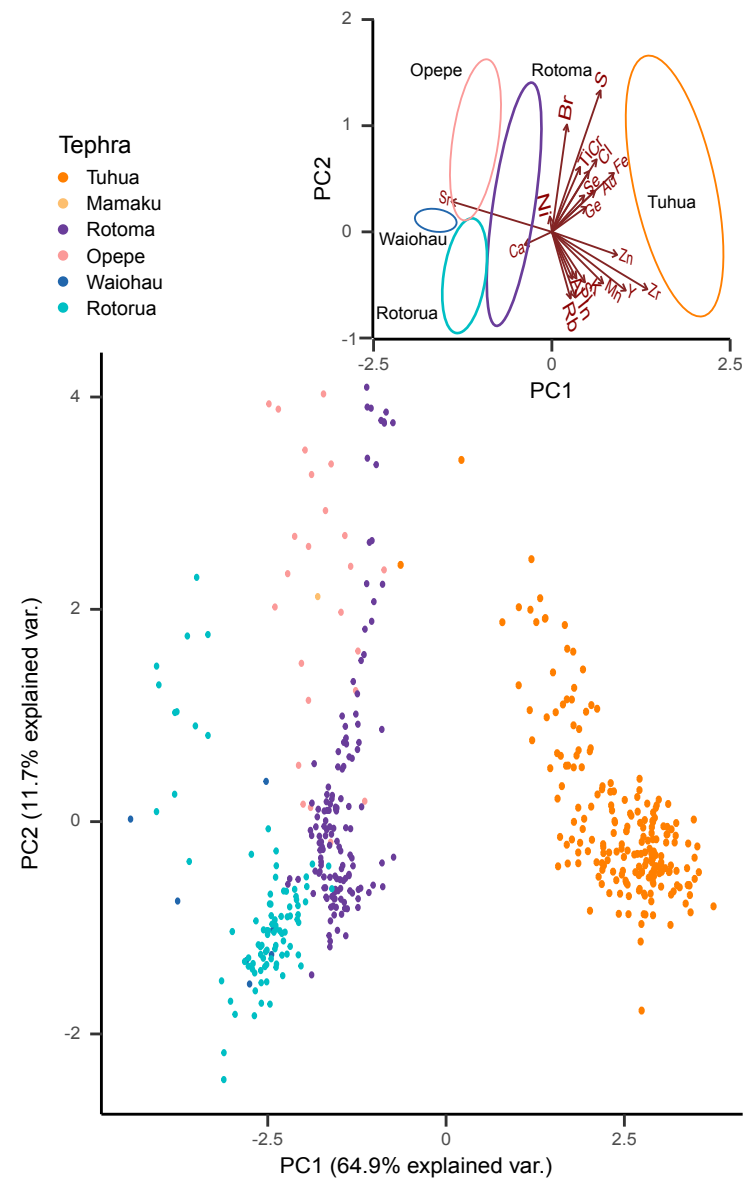
Hopua (measured at Auckland);  
post-KOT; not transformed



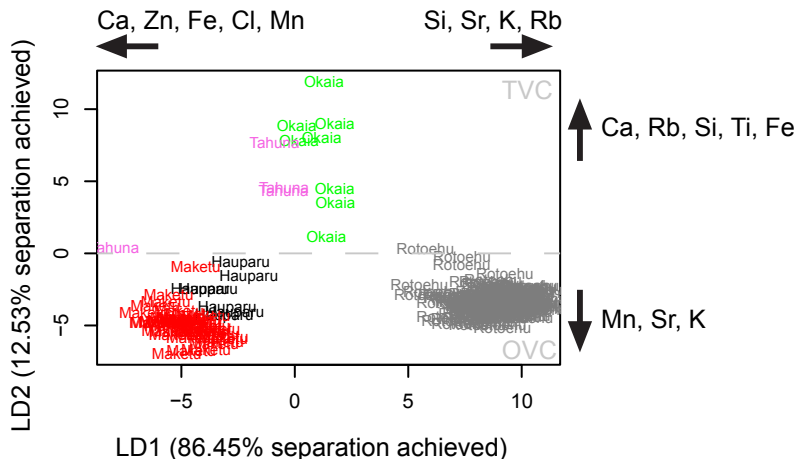
**(A)** Rhyolitic tephra in Onepoto (measured at ANSTO); pre-KOT; log-ratio transformed



**(B)** Rhyolitic tephra in Hopua and Panmure (measured at Auckland); post-KOT; log-ratio transformed



**A**



**B**

